This article was published in Chemical Engineering Journal, 262, 499-508, 2015
http://dx.doi.org/10.1016/j.cej.2014.09.125

O_2 mass transfer in an oscillatory flow reactor provided with smooth periodic constrictions. Individual characterization of k_L and a

A. Ferreira[*,a,b], J.A. Teixeira[a], F. Rocha[b]

[a] *CEB - Centre of Biological Engineering, University of Minho, 4710-057 Braga, Portugal*
[b] *LEPABE-Laboratory for Process Engineering, Environment, Biotechnology and Energy, Departamento de Engenharia Química, Faculdade de Engenharia, Universidade do Porto, Rua Dr. Roberto Frias s/n, 4200-465 Porto, Portugal*

Abstract

In the present work the superficial gas velocities (u_G) and the oscillatory conditions (frequency and amplitude) effects on the gas-liquid mass transfer process in a novel oscillatory flow reactor provided with smooth periodic constrictions (OFR-SPC) are experimentally evaluated. The liquid-side mass transfer coefficient, k_L, and the specific interfacial area, a, are studied individually. The specific interfacial area is obtained using the new automatic image analysis technique developed by Ferreira et al. [1]. The experimental results of volumetric liquid side mass transfer coefficient (k_La), Sauter mean diameter (d_{32}) and gas holdup (ε_G), and the calculated values of a and k_L, are correlated with the superficial gas velocity and the power density (P/V), in order to be used in scale-up processes and in comparisons with the literature. The results show that k_La increases with both superficial gas velocity and oscillatory conditions, the last ones having the highest impact on the

[*]Corresponding author: Tel: + 351 225081678; Fax: + 351 225081632
Email address: amaf@fe.up.pt (A. Ferreira)

mass transfer process. The increase in the oscillation motion (frequency and amplitude) results in bubble size reduction (from $\sim$ 7 mm, without oscillation, to $\sim$ 1 mm, with oscillation), in bubble average residence time increase and, consequently, in a increase. A k_L increase with d_{32} decrease is observed, showing the importance of hydrodynamic phenomena on k_L, specially, when very low bubbles sizes are presented in oscillatory flow reactors.
Key words: Oscillatory flow reactor, Multiphase reactors, Mass transfer, Liquid-side mass transfer coefficient, Specific interfacial area

---

1. Introduction

Multiphase contactors are intensively used in chemical and biological processes. Gas-sparged stirred tanks, air-lift and bubble columns are the most commonly used devices for enhancing gas-liquid mass transfer [2–7]. Nevertheless, problems related with bad mixing, specially when a solid phase is present, product quality, process reproducibility and scale up, are typically reported. In order to overcome some of these limitations oscillatory flow reactors (OFR) have been explored [7–12]. OFR is basically a column provided with periodic constrictions (baffles, with variable geometric configuration, the annular being the most common one), operating under oscillatory flow mixing (OFM). The liquid or multiphase fluid is typically oscillated in the axial direction by means of diaphragms, bellows or pistons, at one or both ends of the tube, developing an efficient mixing mechanism where fluid moves from the walls to the center of the tube with intensity controlled by the oscillation frequency (f) and amplitude (x_0) [13–17]. The formation and dissipation of eddies inside the OFR has proved to result into significant en-

hancement in processes such as mass transfer (see Table 1), heat transfer [18], particle mixing and separation [19], among others. Furthermore, the OFR is also characterized by its linear scale-up [10, 15, 20, 21], minimizing, by this way, the problems related with scale increase. The singular characteristics reported place OFR in line with the process intensification that is a major driving force for reactor engineering [22, 23].

In last years a new generation of OFR has been arising, the meso-OFR. These mesoscale (millilitre) oscillatory baffled reactors have received considerable attention due to their small volume and ability to operate at low flow rates, reducing reagent requirements and waste. Several tube diameters and baffle designs have been tested in order to obtain the best mixing [24–29]. Reis et al.[30–32] used for the first time meso-OFR for gas-liquid mass transfer intensification, in order to be applied in biological processes. The meso-OFR used by the authors has a total volume of 4 mL, an internal diameter of 4.4 mm, and is based on Smooth Periodic Constrictions (SPCs) (see Figure 1), reducing, by this way, the high shear regions that may be crucial for biological processes. Flow patterns within this proposed SPC geometry were found to be very dependent of both x_0 and f, as a result of a controlled fluid convection and dispersion within the SPC tube through vortex rings detachment[24, 33]. Scale-up studies of the meso-OFR were performed by Zheng and Mackley [37] without the presence of gas, in order to establish certain process characteristics of the system. The advantages associated with the use of the SPC geometry in meso-OFR for biotechnological processes [34] and crystallization [35, 36] have been demonstrated.

Despite the previous studies, the application of OFR based on SPC, here-

inafter OFR-SPC, still poorly explored in multiphase systems and limited to one SPC geometry and internal tube diameter (4.4-5 mm). The authors of the present work have been exploring the influence of several geometric parameters that characterize the OFR-SPC (Figure 1) such as: internal tube diameter (D); internal tube diameter in the constrictions (d_o); mean spacing between consecutive constrictions ($L = L_1 + L_2$); constriction length (L_1); straight tube length (L_2); radius of curvature of the sidewall of the convergent subsection (R_c); radius of curvature of the sidewall of the divergent subsection (R_d); radius of curvature of constriction center (R_t); and baffle free cross-sectional area (α), defined as $(d_0/D)^2$, operating in continuous and batch modes. The optimal geometrical parameters for obtaining the lowest mixing times in such OFR were submitted for patent protection, this being the reason of dimensions absence in Figure 1. Nevertheless, the present work explores for the first time the use of a OFR-SCP in gas-liquid mass transfer experiments out of the mesoscale in order to study the SPC influence on hydrodynamic and mass transfer phenomena on a different scale and to identify the differences between the OFR-SPC and the conventional OFR provided with annular baffles, using similar operational conditions. In this sense, the individual contributions of the liquid-side mass transfer coefficient k_L and specific interfacial area, a, on k_La obtained in the novel OFR-SPC are explored. For that, mass transfer results were combined with the specific interfacial area values obtained using the new automatic image analysis technique developed by Ferreira et al. [1].

The methodology adopted on the present work aims to open new insights for a better understanding of mass transfer phenomena in the OFR and

explore the SPC baffle design as an alternative to the conventional annular baffles.

[Table 1 about here.]

2. Experimental facilities and procedure

2.1. Experimental apparatus and operating conditions

Mass transfer experiments were performed in the new oscillatory flow reactor provided with smooth periodic constrictions (OFR-SPC) made of glass (Fig. 1). The reactor inner diameter is ∼2 cm and has 50 cm in height providing a total volume of ∼ 120 mL. The SPC dimensions are not presented, these being under patent protection. Temperature was regulated by a water jacket and a thermostatic bath, maintained at 25 °C.

The fluid was oscillated and aerated using a new oscillatory device, purposely designed, and also under patent protection. The integrated mixing chamber, gas distributor and the capability to be totally thermostatized characterize this device. Oscillation amplitudes (x_0) and frequencies (f) ranged from 0.07 to 0.34 $\times$ L and 1 to 4 Hz, respectively. Values of the amplitudes correspond to the center-to-peak amplitude and these measurements were performed in the tube without constrictions. Superficial gas velocities, u_G, range from 0.1 to 10 mm/s.

The fluid mechanical condition in the OFR is controlled by the oscillatory Reynolds number (Re_o) and the Strouhal number (St), defined as:

$$Re_o = \frac{2\pi f x_0 \rho D}{\mu} \tag{1}$$

$$St = \frac{D}{4\pi x_0} \tag{2}$$

where ρ is the fluid density and μ is the fluid viscosity. The Re_o describes the intensity of mixing applied to the column, and St characterize the effective eddy propagation. According to the operating conditions used Re_o present values corresponding to the laminar, transition and turbulent flow regimes, and St values up to 0.5.

[Figure 1 about here.]

2.2. Mass transfer experiments - Methodology

Oxygen mass transfer experiments were performed in two-phase system at constant temperature (25 °C) and different superficial gas velocities (up to 10 mm/s) controlled by precision gas mass flow controllers (Alicat scientific). Destilled water and Air K were used as liquid and gas phase, respectively. The liquid height was $h_0 = 0.45\ m$ for all experiments (no liquid throughput).

Initially the liquid is deoxygenated by bubbling nitrogen. When the dissolved oxygen concentration is practically zero, air is fed into the column. At this moment the oxygen transfer process from bubbles to the liquid begins and continues until oxygen concentration in the liquid reaches the saturation. Dissolved oxygen concentration values were measured online using an fiberoptic oxygen meter (OXR50-HS, Pyroscience), located 0.35 m from the gas sparger and 0.5 D from the wall, connected to the FireSting O_2 instrument (Pyroscience), and recorded directly in a PC, through the FireSting Logger software. No bubbles interference on the probe measurements was observed. By this way, the dissolved oxygen concentration variation with

time, t, is obtained, and k_La can be calculated according to the following procedure.

The mass balance for oxygen in the liquid is written as:

$$\frac{dC}{dt} = k_La\,(C^* - C) \tag{3}$$

where C^* and C are, respectively, the oxygen solubility and oxygen concentration in the liquid. Assuming the liquid phase homogeneous and C_0 the oxygen concentration at $t = 0$, the integration of the previous equation leads to:

$$\ln\,(C^* - C) = \ln\,(C^* - C_0) - k_La \cdot t. \tag{4}$$

The volumetric mass transfer coefficient can now be determined by plotting $ln(C^* - C)$ against time (t).

Typically, the dissolved oxygen concentration during the aeration has two distinguished zones, one with an intense mass transfer zone where the O_2 concentration rises fast and other close to the saturation, when the mass transfer rate starts to decline. As previously mentioned, plotting $ln(C^* - C)$ against time, k_La can be determined from the slope in the linear zone. In order to define this zone by a statistic way, the statistical method *Test F*[38] was used. This method consists in the determination of the optimum number of points (n_p) for a linear regression of experimental data [39]. The solubility of oxygen in water (C^*) was taken experimentally for each run.

The experimental results are reproducible with an average relative error of 5% and are not influenced by the dynamics of the oxygen electrode since its response time, less than 0.8 s for a 90% confidence interval (technical data), was much smaller than the mass transfer time of the system (ranging

from 4 to 800 s). The claimed average relative error of 5% was calculated from five runs (at same experimental conditions).

2.3. Bubble size distribution and mean bubble size

In order to obtain the bubble size distribution a Perspex rectangular box was fitted at mid-height of the OFR-SPC and filled with water, as shown in Fig. 1. This box minimizes the optical distortion of the OFR-SPC wall curvature. Sets of images were grabbed with a black and white high speed digital video camera (frame rate of 250 images/s) connected to a PC, in the same conditions of k_La determinations. After the acquisition a set of images (about 5 images/s) are automatically treated and the bubbles are identified and classified according to the methodology developed by Ferreira et al. [1]. With the previous methodology, the automatic identification of single bubbles (isolated bubbles without influence of surrounded bubbles) at different operational conditions was possible. The automatic and correct characterization of the single bubbles allows the correct determination of bubble size and, consequently, the specific interfacial area a.

As the shape of the bubbles is influenced by the superficial velocity and oscillatory conditions, the correct determination of bubble size, using image analysis techniques, depends on the bubble shape factor (here defined as $P^2/(4\pi A_{proj})$, where P is the perimeter and A_{proj} the projected bubble area). By this way, this factor was calculated for all single bubbles identified at different experimental conditions. An average value of 1.08 with a variance square root of 0.06 was obtained, indicating by this way that the bubbles produced are, mostly, closed to the spherical geometry. So, the size of each individual bubble (D_{eq_i}) was quantified from the projected bubble

area according to the following equation:

$$D_{eq_i} = \sqrt{\frac{4.A_{proj_i}}{\pi}} \tag{5}$$

For processes involving mass transfer through an interfacial area, the bubble size distribution (BSD) is well represented by the Sauter mean diameter (d_{32}) which is given by

$$d_{32} = \frac{\sum_i n_i \cdot D_{eq_i}^3}{\sum_i n_i \cdot D_{eq_i}^2} \tag{6}$$

2.4. Gas holdup and specific interfacial area

The volume fraction of the gas phase (gas holdup, ε_G) was measured by recording the changes in the liquid height in the OFR-SPC using a high speed digital video camera together with a fine scale fixed on the top of the column. The procedure involves measuring the liquid level without the presence of gas, h_0, and the corresponding level, h, when gas is continuously introduced in the column at a given flow rate and oscillatory conditions (x_0 and f). In order to reduce the error associated to the h measurement an average of 10 values was used for all experimental conditions. The gas holdup is calculated from the volume variation by the following equation:

$$\varepsilon_G = \frac{h - h_0}{h} \tag{7}$$

The relative error associated to the ε_G measurements is less than 10%. The claimed error is the upper limit for voidage error in the range measured. The liquid layer can be located with precision of 0.5 mm (resolution of the scale). For layers with liquid height (h) $\approx$ 45.5-50.1 cm (voidage 1.1-10.2%),

an error of 0.11-0.10% in h is obtained, which causes an error of 10-1%, respectively, in ε_G. The previous methodology was used in u_G range from 2 to 10 mm/s. For smaller u_G, ranging from 0.1 to 1 mm/s, a monofiber optical probe ("Type 1C Probe", A2 Photonic Sensors Ltd., Grenoble, France)[40–42] was used. The ε_G values obtained by this technique were used just as indicative and not as absolute values, as the gas holdup obtained by this technique is a local measurement that can change with probe position (study not performed in this column, but it is not expected a significant variation based on the tube diameter), and be influenced by the oscillatory flow.

Based on gas holdup, ε_G, and the BSD measurements the specific interfacial area, a, was determined as follows:

$$a = 6\frac{\varepsilon_G}{d_{32}} \tag{8}$$

2.5. Power density estimate

In the present work the parameters k_La, k_L, a, ε_G and d_{32} were correlated with the power density, P/V (W m^{-3}), in order to be possible its use in scale-up processes and in comparisons with the literature. The power density, i.e. power consumed per unit volume, in an OFR can be estimated by using the quasi-steady flow model [8, 43],

$$\left(\frac{P}{V}\right)_O = \frac{2\rho N_b}{3\pi C_D^2}\frac{1-\alpha^2}{\alpha^2}x_0^3\omega^3 \tag{9}$$

where ρ is the fluid density (kg m^{-3}), N_b the number of baffles per unit length (m^{-1}), C_D the orifice discharge coefficient (taken as 0.7), α the baffle free cross-sectional area defined as $(d_0/D)^2$, x_0 the oscillation amplitude (m),

and ω the angular frequency of oscillation defined as $2\pi f$. In addition to the external power supplied to the OFR, the specific power dissipation due to rising bubbles in a gas-liquid system was also considered in the present work, following the suggestions of other works [8, 44, 45]. This term is given by

$$(P/V)_B = \rho g u_G \tag{10}$$

where g is the gravitational constant (m s^{-2}) and u_G the superficial gas velocity (m s^{-1}). Therefore, in gas-liquid systems, the overall time-averaged power density is given by

$$P/V = (P/V)_O + (P/V)_B \tag{11}$$

3. Results and discussion

3.1. Bubble size distribution and mean bubble size

The bubble behavior in a baffled column, where an oscillatory motion is applied, is characterized by different phenomena, bubble coalescence and breakage, bubble velocity reduction and bubble trap within each baffled-cell being the most significant. The prevalence of one over another depends of the operating conditions. Fig. 2 shows the effect of the operating conditions, resulting in different fluid mechanical conditions, on the Sauter mean bubble diameter. As it is observed, at low oscillation levels (low x_0 and f - Fig. 2 (a)), the laminar flow regime ($Re_o < 2300$) prevails and the bubble sizes are mainly influenced by the superficial gas velocity, the highest bubble sizes being the ones obtained at higher superficial gas velocities. A particular phenomenon is observed when very low superficial gas velocities

($< 1 \times 10^{-4}$ m/s) are used. At these conditions, the Sauter mean diameter increases with the application of oscillatory motion. This behavior is linked to the OFR constrictions associated to low oscillation levels (low amplitudes and frequencies). The low oscillation levels just conduct to a bubble velocities reduction, not sufficient to promote the bubble break. The presence of constrictions in these conditions promotes the bubble coalescence and, consequently, the bubble size increase. This phenomenon is reduced, specially, when the oscillation amplitude increases, evidencing its strong impact on bubble breakage mechanism (Fig. 2 (a)-(c)). Analyzing Fig. 2, it can be seen that oscillation amplitudes and frequencies play a considerable role on bubble size. For high levels of oscillations the turbulent flow regime ($Re_o > 4000$) is predominant and d_{32} is practically independent of the aeration rate. This behaviour is expected as the increase in amplitude and frequency causes an increase in the power density and, consequently in a bubble size reduction. A similar conclusion was obtained by Oliveira and Ni [45].

[Figure 2 about here.]

From the previous discussion, it is clear that both power density and superficial gas velocity affect d_{32}. In order to determine the relationship between these variables the following equation was used, according to Oliveira and Ni [45]:

$$d_{32} = k u_G^m \left(\frac{P}{V}\right)^n \tag{12}$$

where, k, m and n are constants. In order to fit the d_{32} data to the previous equation the curve fitting toolbox of Matlab® R2012a was used. The best fitting obtained was:

$$d_{32}(m) = 14.51 \times 10^{-3} u_G^{0.10} \left(\frac{P}{V}\right)^{-0.22} \quad (13)$$

The average and maximum relative errors obtained were, -1% and $\pm 36\%$, respectively. The previous equation was compared with Oliveira and Ni [44, 45] works (Fig 3).

[Figure 3 about here.]

As one can see the new OFR-SPC presents small bubble sizes in all operation ranges, as a consequence of the new oscillatory unit, provided with gas distributor, and the new baffle geometry. The first one being responsible for the bubble size at low power densities and the second one at high power densities.

3.2. Gas holdup and specific interfacial area

The measurements of gas holdup as a function of superficial gas velocity at different oscillatory conditions are plotted in Figs. 4 (a)-(c). As one can see the gas holdup is influenced by all variables, superficial gas velocity and oscillatory conditions. Increasing the superficial gas velocity results in a ε_G increase. In what concern the oscillatory conditions, it seems that both frequency and amplitude play a crucial role on ε_G, being the effect of oscillation frequency on ε_G more pronounced at high amplitude. Analysing, globally, Figs. 4 (a)-(c) and Fig. 2 it can be concluded that the presence of small bubbles (less than 3 mm) results in a gas holdup increase, this effect being more pronounced at high oscillation levels (high amplitudes and frequencies) where the turbulent flow regime is predominant. Based on the movies visualization,

obtained during the pictures acquisition for bubble size measurements, the previous effect seems to be related with bubble trap within each baffled-cell increasing its radial velocity and, consequently, its average residence time. These observation are in agreement with Oliveira at al. [46, 47] conclusions, using the conventional OFR, i.e. without SPC.

[Figure 4 about here.]

According to the previous discussion, ε_G was correlated with the superficial gas velocity and the power density. By best fitting of the holdup data, the following equation was obtained:

$$\varepsilon_G = 1.2750 u_G^{0.8015} \left(\frac{P}{V}\right)^{0.1347} \tag{14}$$

The average and maximum relative errors obtained were, 2% and ±42%, respectively, the highest errors being associated to the transition regime (high amplitude and low frequencies, Fig 4 (c)). Fig 4 (d) compares the measured gas holdup values with the ones predicted by Eq. 14 and by Oliveira and Ni [44] equation. It can be seen that Eq. 14 represents better the experimental results. This equation was extrapolated for the experimental conditions that results in a gas holdup less than 1%. As, at these conditions the experimental method based on visual observation can not be used (resulting in significant errors), the predicted gas holdups obtained by using the Eq. 14 were compared with the experimental values using the optical probe. As observed, a very good prediction is obtained, indicating, by this way, the possible use of this correlation outside of the experimental ranges used in the present work.

Based on Eq. 8, 13 and 14 the specific interfacial area can now be obtained:

$$a\ (m^{-1}) = 87.87 u_G^{0.70} \left(\frac{P}{V}\right)^{0.35} \tag{15}$$

This correlation indicates that superficial gas velocity and oscillation intensity plays a significant role on a.

3.3. Mass transfer

The effects of oscillation frequencies and amplitudes on the volumetric liquid side mass transfer coefficient at different aeration rates are plotted in Fig.5 (a)-(c). It can be observed that k_La increases with all variables, k_La being strongly dependent on the intensity of mixing applied to the system resulting in different flow regimes. An increase in the oscillation frequency leads to an increases in k_La. This increase is moderated at small oscillation frequencies but becomes more pronounced at higher oscillation frequencies. This effect is enhanced with the oscillation amplitude increase. For higher oscillation amplitudes, the increase in the oscillation frequency results in a much steeper increase in k_La values. This suggests that k_La is more affected by the oscillation amplitudes, since the oscillation amplitude control the length of the eddy generated along the column that has a strong impact on bubble behavior within the OFR-SPC. In addition, according to the previous sections, increasing the oscillation motion results in a bubble size reduction, in a bubble average residence time increase and, consequently, in an interfacial area increase, leading to a k_La increase.

[Figure 5 about here.]

Following the previous discussion k_La was correlated with the superficial gas velocity and the power density. By best fitting of the k_La data, the following equation was obtained:

$$k_La\ (s^{-1}) = 8.016 \times 10^{-2} u_G^{0.616} \left(\frac{P}{V}\right)^{0.393} \tag{16}$$

Fig 5 (d) compares the measured k_La values with the ones predicted by Eq. 16. It can be seen that Eq. 16 represents well the experimental results. The average and maximum relative errors obtained were, -1% and $\pm 40\%$, respectively, the highest errors being associated to the transition regime (high amplitude and low frequencies, Fig 5 (c)). As mentioned in the Introduction section just few studies have been using OFR for O_2 dissolution, operating in batch mode (see Table 2). The equation obtained in the present work was compared with the best results obtained by Oliveira and Ni [12] and Ni et al. [10] using $u_G = 4.24 \times 10^{-3}$ m/s and $u_G = 8.48 \times 10^{-3}$ m/s, respectively, and a reactor diameter of 50 mm (Fig. 6). On average the OFR-SPC presents k_La values 42% and 20% higher than the ones obtained by Oliveira and Ni [12] and Ni et al. [10], respectively. According to the previous sections these results were expected, since an a increase over the common OFR was observed. However, as the a increase results from the bubble size reduction some precautions need to be taken, since a k_L decrease with d_{32} decrease is expected, according to the literature [12].

[Table 2 about here.]

[Figure 6 about here.]

3.4. Liquid-side mass transfer coefficient

According to Calderbank and Moo-Young [48] k_L is independent on the bubble diameter for the regions of "large" and "small" bubbles, in the intermediate transition region k_L increases linearly with d_{32}. When bubbles are small, they behave as rigid spheres, with practically no liquid circulation at the surface, being k_L proportional to $D_L^{2/3}$, where D_L is the gas diffusivity. On the other hand, large bubbles present mobility interfaces and exhibit significant fluid circulation, k_L being a function of $D_L^{1/2}$. In the transition region (1.7 to 7.2 mm, based on Akita and Moo-Young [49] work using water) bubble size starts to influence k_L value. With bubble size increase, the bubble starts to acquire oscillation, improving, by this way, the renewal rate of the liquid film at the interface leading to a k_L increase. Montes et al. [50] show that oscillating bubbles improve the mass transfer due to the variation of the contact times and the concentration profiles surrounding the bubbles. In addition, Martín et al. [51] found that the superficial area reduction, obtained by bubble size increase, can be balanced with the increase of the amplitude of the oscillation.

Several equations have been proposed to quantify the influence of d_{32} on k_L, however, these are limited to others devices. Oliveira and Ni [12] present, for the first time, an expression for the relative dependence of k_L on d_{32} in the OFR (Eq. 17), where, according to the authors, the d_{32} exponent agrees with Akita and Yoshida [49] expression $\left(k_L \sim d_{32}^{1/2}\right)$.

$$k_L = 0.0072 d_{32}^{0.55 \pm 0.11} \tag{17}$$

In the present work, and in analogy with the previous section, k_L was cor-

related with the superficial gas velocity and the power density. So, combining Eq. 16 and Eq. 15 the following equation is obtained:

$$k_L\ (m/s) = 1.52 \times 10^{-4} u_G^{-0.084} \left(\frac{P}{V}\right)^{0.043} \tag{18}$$

This equation was compared with Oliveira and Ni [12] (Eq. 17) and Akita and Yoshida [49] expressions. For that three superficial gas velocities were used (2×10^{-3}, 6×10^{-3} and 10×10^{-3} m/s). These were chosen in order to compare the k_L values obtained using Eq. 18 (a result of several expressions that "best fit" the experimental results), with the ones obtained using directly the experimental results (k_La, ε_G and d_{32}), with all inherent experimental errors. Comparing k_L obtained from the experimental data with the ones predicted by Eq. 18 (Fig 7) it can be seen that Eq. 18 represents well the experimental results, suggesting k_L dependence of u_G and power density.

Fig. 8 shows a plot of k_L in the OFR-SPC, obtained using Eq. 18, as a function of the Sauter mean diameter. From Fig. 8 it can be seen that k_L does not depends only on d_{32} but also on the agitation of the continuous phase and the aeration rate. As the agitation of the continuous phase is increased the bubble break phenomenon starts to increase and consequently a bubble size reduction is observed. These bubbles start to be trapped within each baffled-cell leading, probably, to an increase in the renewal rate of the liquid film at the interface, conducting, by this way, to a k_L increase. The intensity of this phenomenon seems to be affected by the aeration rate. The amount of small bubbles resulting from the power density increase is much greater at high superficial velocities, resulting in a significant influence of one bubble on the mass transfer process of the others. According to Koynov et al. [52]

in bubble swarms, bubbles no longer traveled by themselves, but rather in liquid perturbed by the wakes of neighboring bubbles. The concentration of gas dissolved in the liquid around the bubble in a swarm no longer depended only on the mass transfer from the bubble itself, but also on the mass transfer from the other bubbles in the swarm. These two factors resulted in a decrease in the mass transfer coefficient of the bubble swarm compared with a single bubble. Ferreira et al [1] quantified this influence based on a new parameter called "bubble population complexity degree" (B_{CD}). According to this parameter it is possible to know if a bubble flows alone (low B_{CD}) or in a bubble group (high B_{CD}). According to the authors, systems with different bubble population complexity degrees present different k_L values, the highest being the ones with the lowest B_{CD} values.

The previous conclusions sustain the observations reported in the present work and could be the reason, beyond the experimental errors, of the scattering observed in the k_L values obtained by Oliveira and Ni [12]. The authors just took into account the d_{32} influence on k_L and not the hydrodynamic system. Comparing the present data with the ones predicted by the literature, it is evident that the literature correlations underestimate the k_L values for bubble sizes bellow 3 mm, which are the ones that suffer a more influence of the hydrodynamic conditions, as explained before.

[Figure 7 about here.]

[Figure 8 about here.]

4. Conclusions

The gas-liquid mass transfer process was investigated for the first time in an oscillatory flow reactor (OFR) provided with smooth periodic constrictions (SPC) operating in batch mode. The main purpose of this work was to analyze the effect of smooth periodic constrictions on k_La, identifying the contribution of its individual parameters, k_L and a, on mass transfer process. For that an extensive experimental measurements of k_La, d_{32} and ε_G were performed. These parameters, as well as a and k_L were successfully correlated with the power density, P/V, allowing its possible use in scale-up processes. The results were compared with literature data of OFR provided with annular baffles.

According to the results, the volumetric liquid side mass transfer coefficient increases with both superficial gas velocity and oscillatory conditions, the last ones having the highest impact on the mass transfer process. k_La increases considerably with oscillation frequency and amplitude, the amplitude having the highest effect, since the oscillation amplitude controls the length of the eddy generated along the column, this affecting strongly the bubble behavior within the OFR-SPC. The increase in the oscillation motion (frequency and amplitude) results in a flow regime transition, in a bubble size reduction, in a bubble average residence time increase and, consequently, in an ε_G and interfacial area increase, leading to a k_La increase. d_{32} and ε_G results show that the novel OFR-SPC, connected to the novel oscillatory unit, results in a bubble size reduction (from $\sim$ 7 mm, without oscillation, to $\sim$ 1 mm, with oscillation) and in a gas holdup increase, caused by an increase in the residence time of the bubbles that become trapped within each

baffled-cell, in comparison with the literature data [44, 45]. The simultaneous increase of d_{32} and ε_G results in a significant increase in a.

Based on the measurements of k_La, d_{32} and ε_G, as well as on the correlations obtained for k_La and a it was possible to calculate the liquid-side mass transfer coefficient. In opposite to the literature, k_L does not depends only on d_{32}; the agitation of the continuous phase and the aeration rate seem to have a significant influence on k_L. As the agitation of the continuous phase is increased, the bubble break phenomenon starts to increase and consequently a bubble size reduction is observed. According to the literature [12], it is expected a k_L decrease with d_{32} decrease. However, in the present work this was not observed. This unexpected behaviour seems to be related to the bubble size obtained in present work (less than 3 mm - Oliveira and Ni [12] sustain their conclusion on $d_{32} > 3$ mm). These bubbles (less than 3 mm) are the ones that suffer more influence of the hydrodynamic conditions, being trapped in vortices, this leading, probably, to a increase in the renewal rate of the liquid film at the interface conducting to a k_L increase. The intensity of this phenomenon seems to be affected by the aeration rate. According to the results, k_L decreases with the superficial gas velocity as a result of the influence of the other bubbles on the concentration profiles surrounding the individual bubbles.

In summary, the present work opens new insights for a better understanding of mass transfer phenomena in the OFR and shows that the new OFR-SPC is a good alternative to the conventional OFR provided with annular baffles, presenting higher k_La values as a result of a and k_L increase.

Nomenclature

A_{proj} - Projected bubble area, m^2

A_{sup_i} - bubble superficial area, m^2

a - specific interfacial area, m^{-1}

B_{CD} - bubble population complexity degree, dimensionless

C - oxygen concentration in the liquid, kg/L

C_0 - oxygen concentration in the liquid at $t = 0$, kg/L

C^* - oxygen solubility in the liquid, kg/L

C_D - orifice discharge coefficient (taken as 0.7), dimensionless

D - inner diameter of the straight section, m

D_{eq} - equivalent diameter, m

D_L - diffusivity of gas in the liquid, m^2/s

d_0 -internal tube diameter in the constrictions, m

d_{32} - Sauter mean diameter, m

f - oscillation frequency, Hz

g - gravitational constant, m s^{-2}

H - column height, m

h - liquid height, m

h_0 - initial liquid height, m

k - constants of Eq.13, dimensionless

k_L - liquid-side mass transfer coefficient, m/s

k_La - volumetric liquid side mass transfer coefficient, s^{-1}

L - mean spacing between consecutive constrictions, m

L_1 - constriction length, m

L_2 - straight tube length, m

m - constants of Eq.13, dimensionless

n - constants of Eq.13, dimensionless

N_b - number of baffles per unit length, m^{-1}

n_p - number of points, dimensionless

P - perimeter, m

P/V - power density, W m^{-3}

R_c - radius of curvature of the sidewall of the convergent subsection, m

R_d - radius of curvature of the sidewall of the divergent subsection, m

R_t - radius of curvature of constriction center, m

T - temperature, °C

t - time, s

u_G - superficial gas velocity, m/s

x_0 - oscillation amplitude, m

α - baffle free cross-sectional area defined as $(d_0/D)^2$, dimensionless

μ - fluid viscosity, kg m^{-1} s^{-1}

ω - angular frequency of oscillation defined as $2\pi f$, Hz

ρ - fluid density, kg m^{-3}

ε_G - gas holdup, dimensionless

Acknowledgements

This work was supported by Fundação para a Ciência e Tecnologia under program contract number SFRH/BPD/45637/2008.

References

[1] A. Ferreira, G. Pereira, J. Teixeira, F. Rocha, Statistical tool combined with image analysis to characterize hydrodynamics and mass transfer in a bubble column, Chem. Eng. J. 180 (2012) 216–228.

[2] B. Smith, D. Skimore, Mass Transfer Phenomena in an Airlift Reactor: Effects of Solids Loading and Temperature, Biotechnol. Bioeng. 35 (1990) 483–491.

[3] W. D. Deckwer, Bubble Column Reactors, J. Wiley.

[4] V. Linek, M. Kordac, M. Fujasová, T. Moucha, M. Korda, Gas-liquid mass transfer coefficient in stirred tanks interpreted through models of idealized eddy structure of turbulence in the bubble vicinity, Chem. Eng. and Process. 43 (12) (2004) 1511–1517.

[5] A. S. Mirón, M.-C. C. García, F. G. Camacho, E. M. Grima, Y. Chisti, Mixing in bubble column and airlift reactors, Chem. Eng. Res. Des. 82 (A10) (2004) 1367–1374.

[6] J. Sánchez Pérez, E. Rodríguez Porcel, J. Casas López, J. Fernández Sevilla, Y. Chisti, Shear rate in stirred tank and bubble column bioreactors, Chem. Eng. J. 124 (1-3) (2006) 1–5.

[7] M. S. R. Abbott, A. P. Harvey, G. V. Perez, M. K. Theodorou, Biological processing in oscillatory baffled reactors : operation , advantages and potential, Inter Focus 3 (December 2012).

[8] R. Hewgill, M. R. Mackley, A. B. Pandit, S. S. Pannu, Enhancement of gas-liquid mass transfer using oscillatory flow in a baffled tube, Chem. Eng. Sci. 48 (4) (1993) 799–809.

[9] X. Ni, G. S, R. Cumming, P. DW, A Comparative-Study of Mass-Transfer in Yeast for a Batch Pulsed Baffled Bioreactor and a Stirred-Tank Fermenter, Chem. Eng. Sci. 50 (13) (1995) 2127–2136.

[10] X. Ni, S. Gao, Scale-up correlation for mass transfer coefficients in pulsed baffled reactors, Chem. Eng. J. 63 (1996) 157–166.

[11] M. R. Mackley, P. Stonestreet, N. C. Thurston, J. S. Wiseman, Evaluation of a Novel Self-Aerating , Oscillating Baffle Column, Can. J. Chem. Eng. 76 (1) (1998) 5–10.

[12] M. S. N. Oliveira, X.-w. Ni, Effect of hydrodynamics on mass transfer in a gas-liquid oscillatory baffled column, Chem. Eng. J. 99 (2004) 59–68.

[13] M. Mackley, X. Ni, Mixing and dispersion in a baffled tube for steady laminar and pulsatile flow, Chem. Eng. Sci. 46 (12) (1991) 3139–3151.

[14] M. Mackley, X. Ni, Experimental Fluid Dispersion Measurements in Periodic Baffled Tube Arrays, Chem. Eng. Sci. 48 (18) (1993) 3293–3305.

[15] K. B. Smith, The Scale-Up of Oscillatory Flow Mixing, Ph.D. thesis, University of Cambridge (1999).

[16] A. W. Fitch, X. Ni, On the determination of axial dispersion coefficient

in a batch oscillatory baffled column using laser induced fluorescence, Chem. Eng. J. 92 (2003) 243–253.

[17] A. W. Fitch, H. Jian, X. Ni, An investigation of the effect of viscosity on mixing in an oscillatory baffled column using digital particle image velocimetry and computational fluid dynamics simulation, Chem. Eng. J. 112 (1-3) (2005) 197–210.

[18] M. Mackley, P. Stonestreet, Heat-Transfer and Associated Energy Dissipation for Oscillatory Flow in Baffled Tubes, Chem. Eng. Sci. 50 (14) (1995) 2211–2224.

[19] M. Mackley, K. Smith, N. Wise, The Mixing and Separation of Particle Suspensions Using Oscillatory Flow in Baffled Tubes, Chem. Eng. Res. Des. 71 (A6) (1993) 649–656.

[20] H. Jian, X. Ni, A Numerical Study on the Scale-Up Behaviour in Oscillatory Baffled Columns, Chem. Eng. Res. Des. 83 (10) (2005) 1163–1170.

[21] K. B. Smith, M. R. Mackley, An experimental investigation into the scale-up of oscillatory flow mixing in baffled tubes, Chem. Eng. Res. Des. 84 (A11) (2006) 1001.

[22] M. Mackley, Process and product innovation, J. Chem. Technol. Biot. 78 (2-3) (2003) 94–97.

[23] X. Ni, M. R. Mackley, A. P. Harvey, P. Stonestreet, M. H. I. Baird, N. V. R. Rao, Mixing through oscillations and pulsations - a guide to achieving process enhancements in the chemical and process industries, Chem. Eng. Res. Des. 81 (A3) (2003) 373–383.

[24] N. Reis, a.a. Vicente, J. Teixeira, M. Mackley, Residence times and mixing of a novel continuous oscillatory flow screening reactor, Chem. Eng. Sci. 59 (22-23) (2004) 4967–4974.

[25] A. N. Phan, A. Harvey, Development and evaluation of novel designs of continuous mesoscale oscillatory baffled reactors, Chem. Eng. J. 159 (1-3) (2010) 212–219.

[26] A. N. Phan, A. P. Harvey, Effect of geometrical parameters on fluid mixing in novel mesoscale oscillatory helical baffled designs, Chem. Eng. J. 169 (1-3) (2011) 339–347.

[27] A. N. Phan, A. Harvey, J. Lavender, Characterisation of fluid mixing in novel designs of mesoscale oscillatory baffled reactors operating at low flow rates (0.3-0.6ml/min), Chem. Eng. Process. 50 (3) (2011) 254–263.

[28] A. N. Phan, A. P. Harvey, M. Rawcliffe, Continuous screening of base-catalysed biodiesel production using New designs of mesoscale oscillatory baffled reactors, Fuel Process. Technol. 92 (8) (2011) 1560–1567.

[29] A. N. Phan, A. P. Harvey, Characterisation of mesoscale oscillatory helical baffled reactor - Experimental approach, Chem. Eng. J. 180 (2012) 229–236.

[30] N. M. F. Reis, Novel Oscillatory Flow Reactors for Biotechnological Applications, Ph.D. thesis, Minho University (2006).

[31] N. Reis, P. Mena, A. Vicente, J. Teixeira, F. Rocha, The intensification of gas-liquid flows with a periodic, constricted oscillatory-meso tube, Chem. Eng. Sci. 62 (24) (2007) 7454–7462.

[32] N. Reis, R. N. Pereira, A. A. Vicente, J. A. Teixeira, Enhanced Gas-Liquid Mass Transfer of an Oscillatory Constricted-Tubular Reactor, Ind. Eng. Chem. Res. 47 (2008) 7190–7201.

[33] N. Reis, A. Harvey, M. Mackley, A. Vicente, J. Teixeira, Fluid Mechanics and Design Aspects of a Novel Oscillatory Flow Screening Mesoreactor, Chem. Eng. Res. Des. 83 (4) (2005) 357–371.

[34] N. Reis, C. N. Gonc, A. A. Vicente, J. A. Teixeira, Proof-of-Concept of a Novel Micro-Bioreactor for Fast Development of Industrial Bioprocesses, Biotechnol. Bioeng. 95 (4) (2006) 744–753.

[35] F. Castro, A. Ferreira, F. Rocha, A. Vicente, J. A. Teixeira, Continuous-Flow Precipitation of Hydroxyapatite at 37 ° C in a Meso Oscillatory Flow Reactor, Ind. Eng. Chem. Res. 52 (2013) 9816–9821.

[36] F. Castro, A. Ferreira, F. Rocha, A. Vicente, J. A. Teixeira, Precipitation of Hydroxyapatite at 37 C in a Meso Oscillatory Flow Reactor Operated in Batch at Constant Power Density, AIChE J. 59 (12) (2013) 4483–4493.

[37] M. Zheng, M. Mackley, The axial dispersion performance of an oscillatory flow meso-reactor with relevance to continuous flow operation, Chem. Eng. Sci. 63 (7) (2008) 1788–1799.

[38] P. G. Hoel, Elementary Statistics, 4th Edition, John Wiley & Sons Inc., Australia, 1976.

[39] P. Mena, a. Ferreira, J. A. Teixeira, F. Rocha, Effect of some solid

properties on gas-liquid mass transfer in a bubble column, Chem. Eng. and Process. 50 (2) (2011) 181–188.

[40] A. Cartellier, Measurement of Gas Phase Characteristics Using New Monofiber Optical Probes and Real Time Signal Processing, Nucl. Eng. Des. 184 (1998) 393–408.

[41] P. C. Mena, F. A. Rocha, J. A. Teixeira, a. Cartellier, P. Sechet, Measurement of Gas Phase Characteristics Using a Monofiber Optical Probe in a Three-Phase Flow, Chem. Eng. Sci. 63 (16) (2008) 4100–4115.

[42] J. Vejražka, M. Večeř, S. Orvalho, P. Sechet, M. C. Ruzicka, A. Cartellier, Measurement accuracy of a mono-fiber optical probe in a bubbly flow, Int. J. Multiphas Flow 36 (7) (2010) 533–548.

[43] A. C. Jealous, H. F. Johnson, Power requirements for pulse generation in pulse columns, Ind. Eng. Chem. 47 (6) (1955) 1159–1166.

[44] M. S. N. Oliveira, X. Ni, Gas hold-up and bubble diameters in a gassed oscillatory baffled column, Chem. Eng. Sci. 56 (21-22) (2001) 6143–6148.

[45] M. S. N. Oliveira, X.-w. Ni, Characterization of a Gas-Liquid OBC : Bubble Size and Gas Holdup, AIChE J. 50 (12) (2004) 3019–3033.

[46] M. S. N. Oliveira, A. W. Fitch, X. Ni, A study of bubble velocity and bubble residence time in a gassed oscillatory baffled column: Effect of oscillation frequency, Chem. Eng. Res. Des. 81 (2) (2003) 233–242.

[47] M. S. N. Oliveira, A. W. Fitch, X.-w. Ni, A study of velocity and residence time of single bubbles in a gassed oscillatory baffled column: Effect

of oscillation amplitude, J. Chem. Technol. Biotechnol. 78 (2-3) (2003) 220–226.

[48] P. H. Calderbank, M. B. Moo-Young, The continuous phase heat and mass-transfer properties of dispersions, Chem. Eng. Sci. 16 (1-2) (1961) 39–54.

[49] K. Akita, F. Yoshida, Bubble Size, Interfacial Area, and Liquid-Phase Mass Transfer Coefficient in Bubble Columns, Ind Eng Chem Process Des Dev 13 (1) (1974) 84–91.

[50] F. Montes, M. Galan, R. Cerro, Mass transfer from oscillating bubbles in bioreactors, Chem. Eng. Sci. 54 (15-16) (1999) 3127–3136.

[51] M. Martín, F. J. Montes, M. A. Galán, Bubble coalescence at sieve plates: II. Effect of coalescence on mass transfer. Superficial area versus bubble oscillations, Chem. Eng. Sci. 62 (6) (2007) 1741–1752.

[52] A. Koynov, J. G. Khinast, G. A. Tryggvason, Mass transfer and chemical reactions in bubble swarms with dynamic interfaces, AIChE J. 51 (10) (2005) 2786–2800.

List of Figures

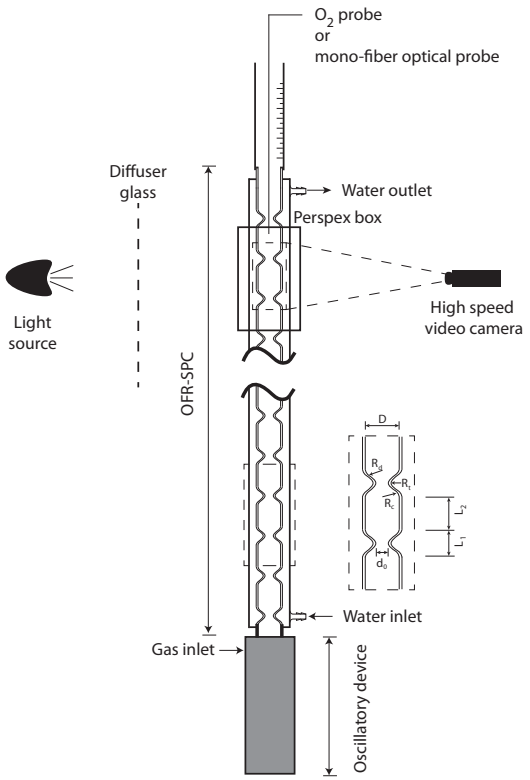

Figure 1: Schematic diagram of the experimental apparatus. D - inner diameter of the straight section; d_0-internal tube diameter in the constrictions; L_1 - constriction length; L_2 - straight tube length; R_c - radius of curvature of the sidewall of the convergent subsection; R_d - radius of curvature of the sidewall of the divergent subsection; R_t - radius of curvature of constriction center.

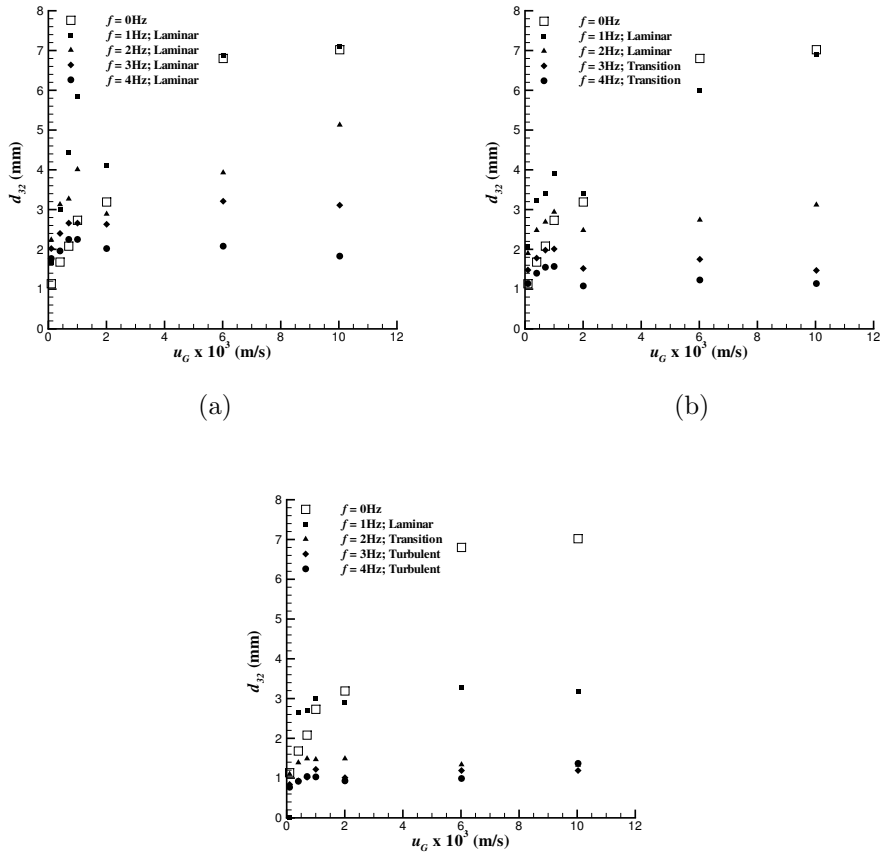

Figure 2: Effect of oscillation frequency and superficial gas velocity on Sauter mean diameter in the OFR-SPC using different amplitudes: (a) $x_o = 0.07 \times L$; (b) $x_o = 0.17 \times L$; (c) $x_o = 0.34 \times L$. Identification of the different flow regimes.

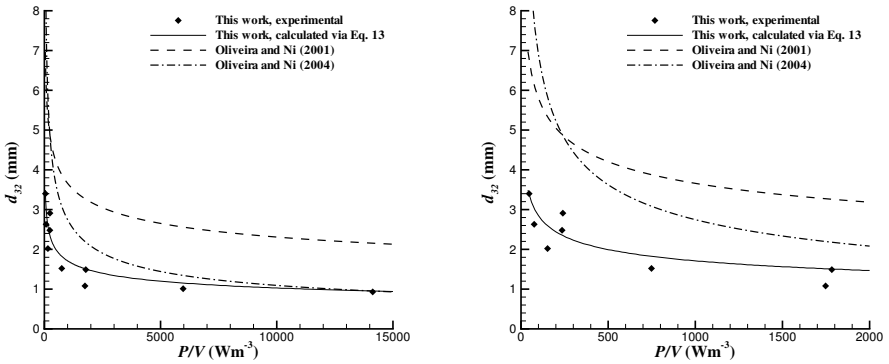

(a) (b)

Figure 3: Effect of power density on Sauter mean diameter at $u_G = 2$ mm/s.

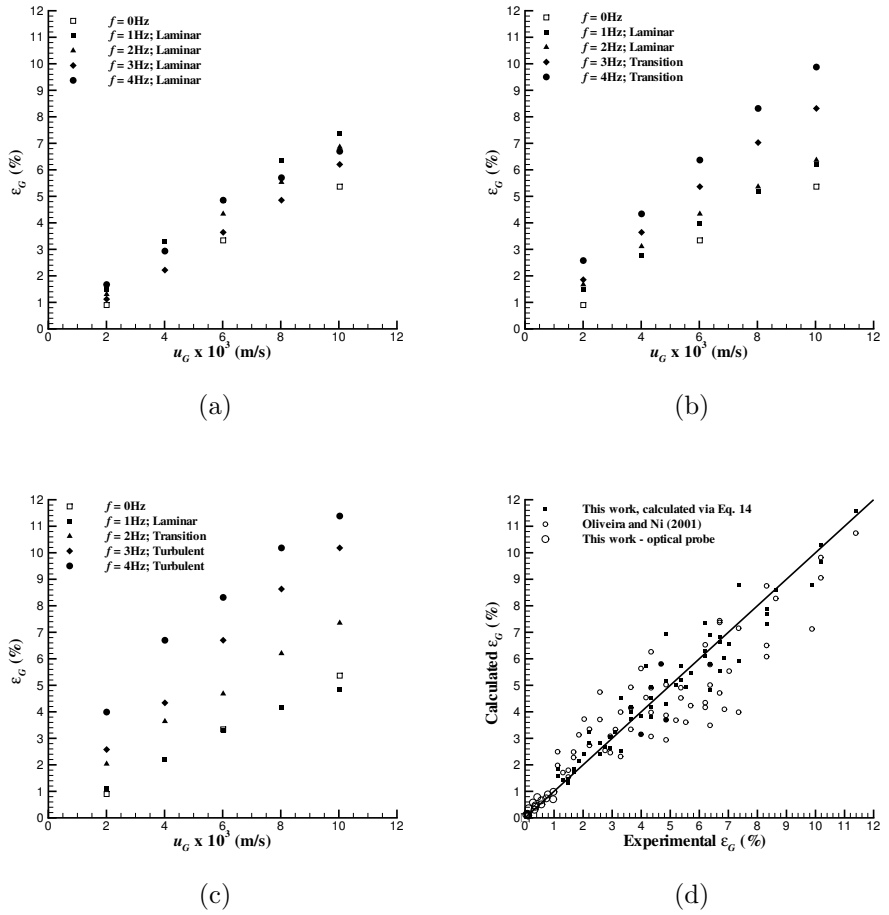

Figure 4: Effect of oscillation frequency and superficial gas velocity on gas holdup in the OFR-SPC using different amplitudes: (a) $x_o = 0.07 \times L$; (b) $x_o = 0.17 \times L$; (c) $x_o = 0.34 \times L$; (d) experimental and calculated gas holdup using Eq.14. Identification of the different flow regimes.

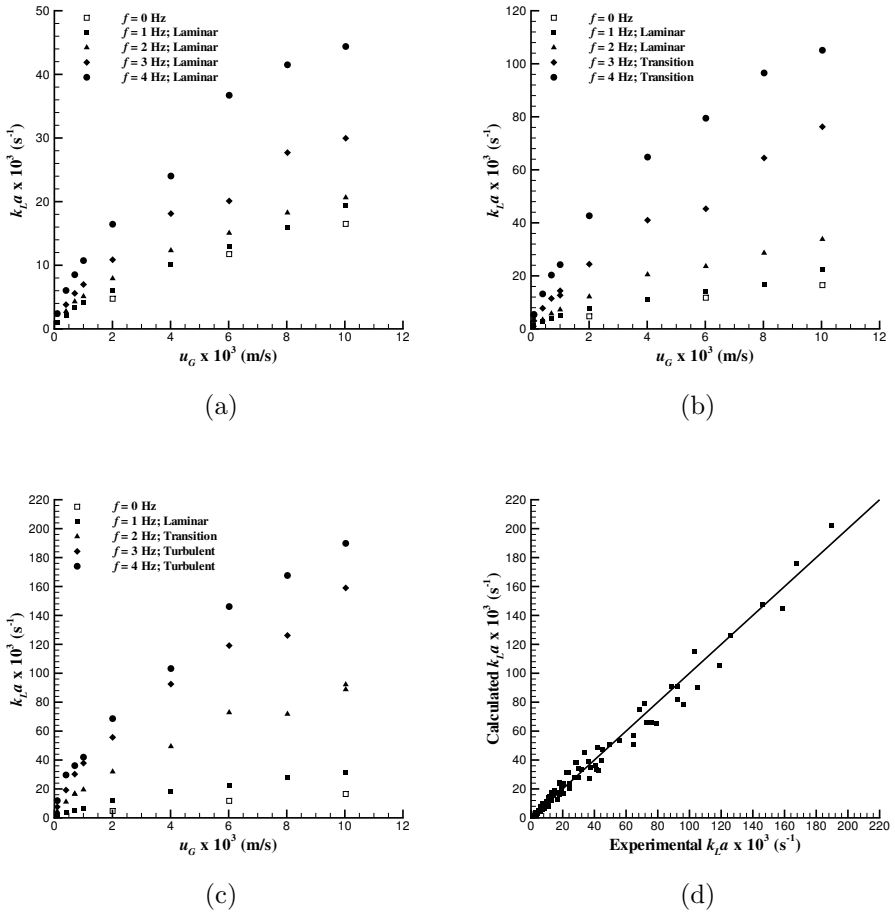

Figure 5: Effect of oscillation frequency and superficial gas velocity on volumetric liquid side mass transfer coefficient in the OFR-SPC using different amplitudes: (a) $x_o = 0.07 \times L$; (b) $x_o = 0.17 \times L$; (c) $x_o = 0.34 \times L$; (d) experimental and calculated $k_L a$ using Eq. 16. Identification of the different flow regimes.

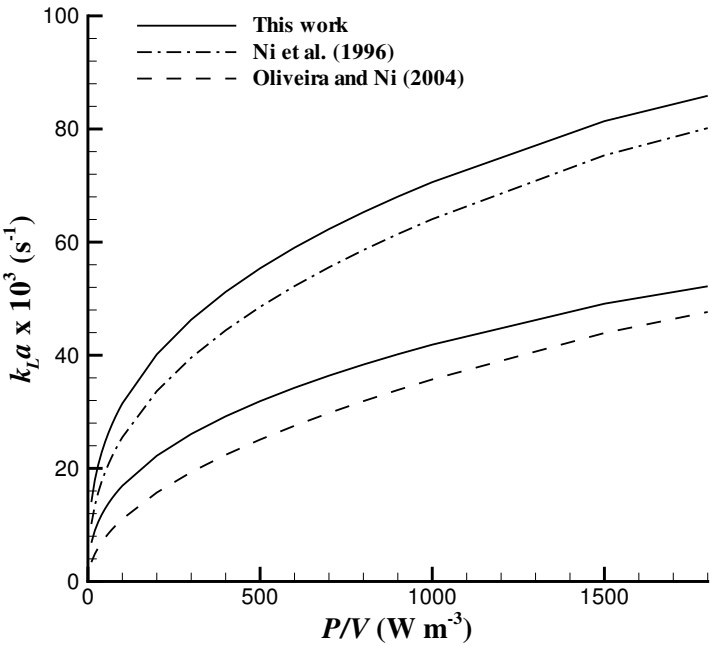

Figure 6: Effect of power density on volumetric liquid side mass transfer coefficient using the OFR-SPC and the common OFR - Oliveira and Ni [12] using $u_G = 4.24 \times 10^{-3}$ m/s and Ni et al. [10] using $u_G = 8.48 \times 10^{-3}$ m/s.

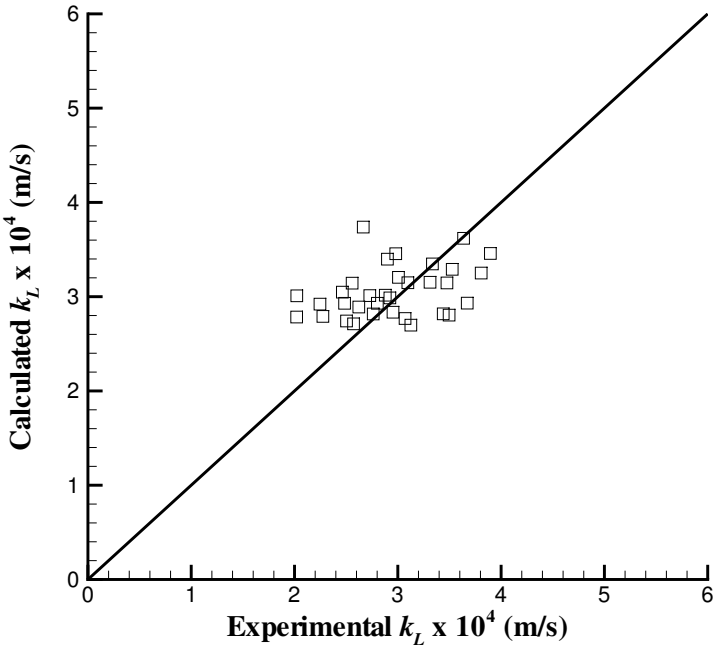

Figure 7: Calculated k_L using Eq.18 and the experimental data (k_La, ε_G and d_{32}).

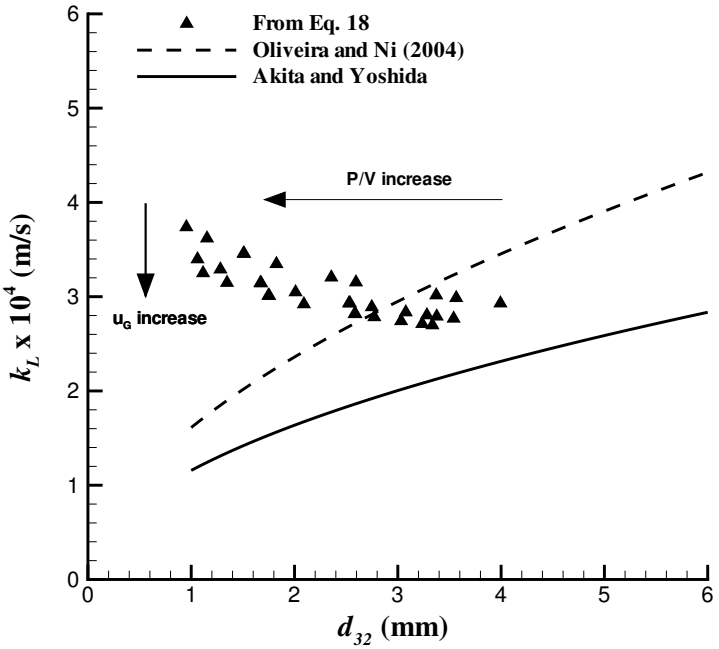

Figure 8: Effect of Sauter mean diameter on k_L calculated using Eq.18 and the expressions of Oliveira and Ni [12] (Eq. 17) and Akita and Yoshida [49].

List of Tables

Table 1: Gas-liquid mass transfer studies in oscillatory baffled columns at batch conditions.

Reference	D (mm)	d_0 (mm)	H (mm)	α	$u_G\mathbf{x}\ 10^3$ (m/s)	k_La (s^{-1})
Hewgill et al.[8]	26	15	750	33	0.42-2.40	up to 0.037
Ni et al. [9]	50	23	400	21	3.2	∼0.025-0.125
Ni et al. [10]	50	23	375	21	2.12-8.48	up to 0.14
Ni et al. [10]	100	46	875	21	4.24-16.96	up to 0.13
Mackley et al. [11]	190	10-50	∼1000	7-31	-	up to 0.007
Oliveira et al. [12]	50	24	1500	23	1.06-4.24	up to 0.039

Table 2: Mass transfer coefficient correlations for gas-liquid oscillatory baffled columns.

Reference	Correlation (s^{-1})	P/V (W/m^3)
Hewgill et al. [8]	$k_La = 1.22\left(\frac{P}{V}\right)^{0.32} u_G^{0.94}$	< 600
Ni et al. [10] (D=50 mm)	$k_La = 0.0186\left(\frac{P}{V}\right)^{0.4} u_G^{0.32}$	32-7021
Ni et al. [10] (D=100 mm)	$k_La = 0.0256\left(\frac{P}{V}\right)^{0.425} u_G^{0.37}$	32-1488
Oliveira and Ni [12]	$k_La = 0.043 \frac{e_g^{1\pm0.07}}{D_{32}^{0.45\pm0.11}}$	10-1700